Supplemental material

Gamal El-Din et al., https://doi.org/10.1085/jgp.201711884

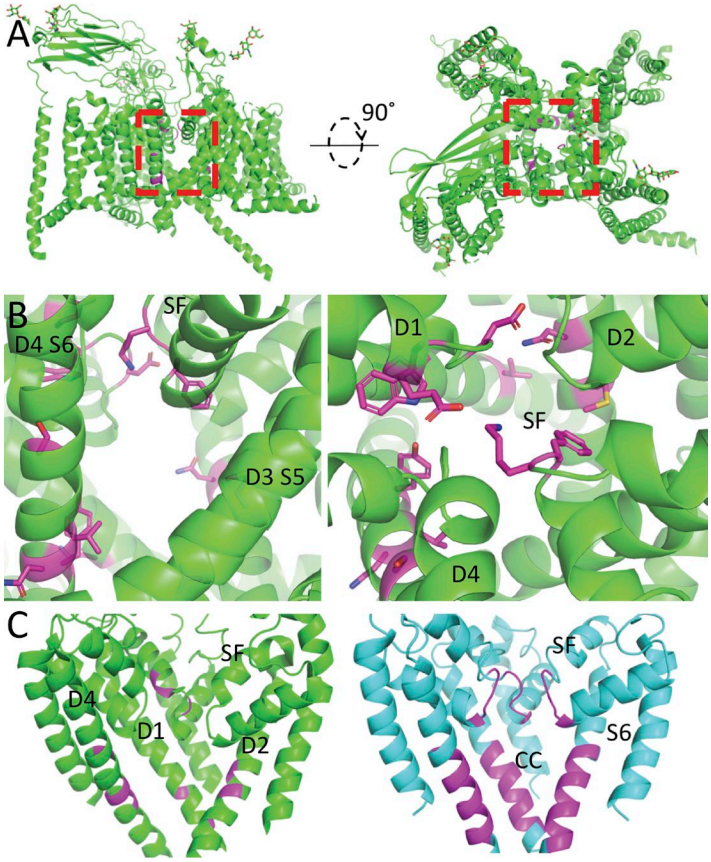

Figure S1. **Residues involved in slow inactivation of mammalian Na_V channels compared with Na_VAb regions that change conformation during adoption of its putative slow inactivated state. (A)** Orthogonal views of the overall fold of $Na_V1.4$ from electric eel, as determined by cryo-EM (PDB accession no. 5XSY). Residues shown to affect mammalian slow inactivation have been highlighted in magenta (see also Table S1). **(B)** Close-up view of the red boxes shown in A, with residues from Table S1 shown in stick format. Left: View of the central cavity as if the viewer is standing in the fenestration between domain 3 (D3) and domain 4 (D4) of $Na_V1.4$. Right: View of the protein as if the viewer is standing above the channel and looking downward through the selectivity filter (SF) and permeation pathway. D, domain. **(C)** A view of $Na_V1.4$ (left, green) and Na_VAb (right, cyan) with one of four monomers and voltage sensors removed in order to highlight residues involved in slow inactivation of eukaryotic (left, magenta) and prokaryotic channels (right, magenta). We have used homology to map involved residues (highlighted in magenta, listed in Table S1) onto $Na_V1.4$.

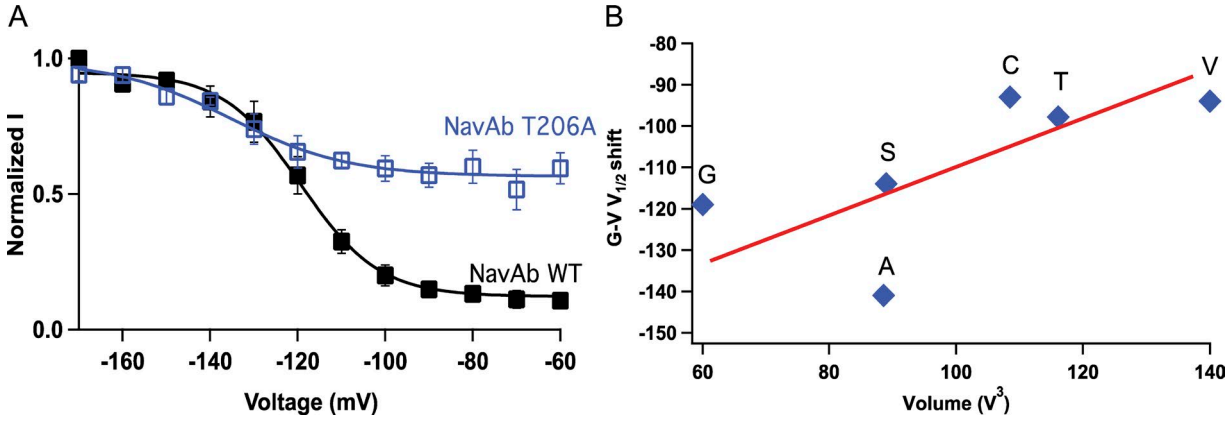

Figure S2. **Effects of Thr206 mutations on voltage dependence of steady-state early inactivation and voltage dependence of activation. (A)** Steady-state inactivation curves for T206A and Na_VAb/WT. **(B)** Midpoints ($V_{1/2}$) of G–V curves for constructs with the indicated amino acid residues at position 206 plotted as a function of side-chain volume. Error bars represent SEM.

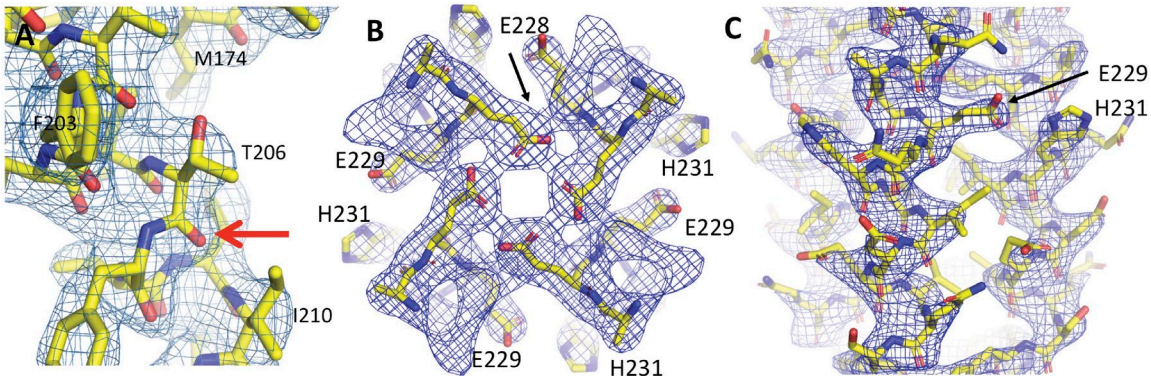

Figure S3. **Electron density maps of the S6 helix at Thr206 and the C-terminal coiled-coil motif. (A)** A simulated annealing omit map is shown for $Na_VAb\Delta28$. The map was calculated with omission of residues Ile202 through Leu212 and is contoured at 1.0 sigma in stick format. Arrow highlights the main chain carbonyl at Thr206 to show the high quality of our electron density measurements at this resolution. **(B and C)** Exemplar electron density is shown for $Na_VAb\Delta28$ in orthogonal views. Left: Four-helix bundle and key intersubunit hydrogen bonds at the level of Glu228, Glu229, and His231. A 2fo-fc electron density map shown at 1.0 sigma as blue mesh, and selected side chains are shown in stick format. Right: Four-helix bundle of the C-terminal domain with maps and protein model as in the left panel.

Table S1. **Structural comparison of early voltage-dependent inactivation of bacterial Na_V channels to slow inactivation in mammalian Na_V channels**

Residue (Na_VAb)	Location	Homolog (eukaryotic Na_V)	References
L176	Selectivity filter	F1236 (rat $Na_V1.4$ D4)	Ong et al., 2000
E177	Selectivity filter	D400, K1237 (rat $Na_V1.4$, D1 and D4)	Todt et al., 1999; Hilber et al., 2005
W179	Selectivity filter	W402 (rat $Na_V1.4$, D1)	Balser et al., 1996
S180	Selectivity filter	E403 (rat $Na_V1.4$, D1)	Xiong et al., 2006
V205	S6 helix	S1579 (human $Na_V1.5$, D4)	Wang et al., 2005
T206	S6 helix	N927 (human $Na_V1.5$, D2)	Chancey et al., 2007
M209	S6 helix	V787 (rat $Na_V1.4$, D2), V930 (human $Na_V1.5$, D2)	O'Reilly et al., 2001; Chancey et al., 2007
I210	S6 helix	V1583 (rat $Na_V1.4$, D4)	Vedantham and Cannon, 2000
N211	S6 helix	N434A, N1466 (rat $Na_V1.4$, D1 and D4)	Wang and Wang, 1997; Chen et al., 2006
V213	S6 helix	Y1586 (rat $Na_V1.4$, D4)	O'Reilly et al., 2000
I216	S6 helix	V445 (human $Na_V1.4$, D1)	Takahashi and Cannon, 1999

The indicated amino acid residues in Na_VAb are listed in the first column, and their locations in the structure are listed in the second column. The analogous amino acid residue in a mammalian Na_V channel is listed in the third column, and references showing the effects of mutation of this amino acid residue on slow inactivation are given in the fourth column. D, domain.

Table S2. **X-ray data collection and refinement statistics**

	$Na_VAb\Delta28$	$Na_VAb28/T206A$	$Na_VAb\Delta28/T206S$	$Na_VAb\Delta28/T206V$
Data collection				
Space group	I422	I422	I422	I422
Unit cell (a, b, c, $\alpha = \beta = \gamma$)	124.772 124.772 189.797 90	123.849 123.849 190.006 90	124.495 124.495 189.669 90	124.175 124.175 189.868 90
R_{meas}[a]	0.105 (>1)	0.123 (>1)	0.097 (>1)	0.101 (>1)
R_{merge}	0.103 (>1)	0.120 (>1)	0.09 (>1)	0.099 (>1)
R_{pim}[b]	0.030 (0.480)	0.044 (0.383)	0.037 (0.667)	0.033 (0.480)
$I/\sigma I$	22.6 (0.5)	22 (1.0)	18.3 (0.5)	24.6 (1.0)
Resolution average $I/\sigma I = 2$	2.64	2.74	2.59	2.59
Completeness (%)	97.4 (79.0)	99.1 (88.7)	97.3 (84.9)	99.8 (98.6)
Redundancy	12.7 (5.3)	9.4 (5.6)	7 (6.0)	11.1 (7.7)
$CC_{1/2}$ (highest shell)[c]	0.581	0.790	0.506	0.862
Refinement				
Resolution (Å)	29.78–2.40 (2.49–2.40)	29.67–2.60 (2.693–2.60)	29.57–2.327 (2.411–2.327)	29.74–2.50 (2.59–2.50)
Reflections	28,621 (2,189)	22,844 (2,075)	30,943 (2,428)	25,875 (2,477)
R_{work}/R_{free}	0.2110/0.2412	0.2031/0.2350	0.2115/0.2457	0.2160/0.2369
Atoms	2,161	2,169	2,188	2,133
Protein/ligand/water	1,927/208/26	1,917/224/28	1,925/239/24	1,898/210/25
B-factor	79.92	83.08	91.15	81.30
Protein/ligand/water	79.4/86.4/67.2	82.0/93.2/76.5	89.45/105.9/80.5	80.48/89.34/76.49
RMSD deviations				
RMSD bonds (Å)	0.007	0.008	0.008	0.008
RMSD angles (degrees)	0.98	1.08	0.84	1.06
MolProbity analysis				
Ramachandran outliers (%)	0.00	0.00	0.00	0.00
Ramachandran favored (%)	98.30	97.86	98.29	97.41
Clash score	8.00	9.33	8.99	10.8
Overall score	2.25	2.24	2.11	2.27

[a]$R_{meas} = \Sigma(N/(N-1))^{1/2} \cdot |I - \langle I \rangle| / \Sigma I$, where N = the number of symmetry related reflections, I = the observed intensity for a reflection, and $\langle I \rangle$ = the average intensity obtained from multiple observations of symmetry-related reflections.
[b]$R_{pim} = \Sigma(1/(N-1))^{1/2} \cdot |I - \langle I \rangle| / \Sigma I$.
[c]$CC_{1/2}$ = The Pearson Correlation Coefficient between intensities calculated from random half datasets.

References

Balser, J.R., H.B. Nuss, N. Chiamvimonvat, M.T. Pérez-García, E. Marban, and G.F. Tomaselli. 1996. External pore residue mediates slow inactivation in mu 1 rat skeletal muscle sodium channels. *J. Physiol.* 494:431–442. https://doi.org/10.1113/jphysiol.1996.sp021503

Chancey, J.H., P.E. Shockett, and J.P. O'Reilly. 2007. Relative resistance to slow inactivation of human cardiac Na+ channel hNav1.5 is reversed by lysine or glutamine substitution at V930 in D2-S6. *Am. J. Physiol. Cell Physiol.* 293:C1895–C1905. https://doi.org/10.1152/ajpcell.00377.2007

Chen, Y., F.H. Yu, D.J. Surmeier, T. Scheuer, and W.A. Catterall. 2006. Neuromodulation of Na+ channel slow inactivation via cAMP-dependent protein kinase and protein kinase C. *Neuron*. 49:409–420. https://doi.org/10.1016/j.neuron.2006.01.009

Hilber, K., W. Sandtner, T. Zarrabi, E. Zebedin, O. Kudlacek, H.A. Fozzard, and H. Todt. 2005. Selectivity filter residues contribute unequally to pore stabilization in voltage-gated sodium channels. *Biochemistry*. 44:13874–13882. https://doi.org/10.1021/bi0511944

O'Reilly, J.P., S.Y. Wang, and G.K. Wang. 2000. A point mutation in domain 4-segment 6 of the skeletal muscle sodium channel produces an atypical inactivation state. *Biophys. J.* 78:773–784. https://doi.org/10.1016/S0006-3495(00)76635-5

O'Reilly, J.P., S.Y. Wang, and G.K. Wang. 2001. Residue-specific effects on slow inactivation at V787 in D2-S6 of Na(v)1.4 sodium channels. *Biophys. J.* 81:2100–2111. https://doi.org/10.1016/S0006-3495(01)75858-4

Ong, B.H., G.F. Tomaselli, and J.R. Balser. 2000. A structural rearrangement in the sodium channel pore linked to slow inactivation and use dependence. *J. Gen. Physiol.* 116:653–662. https://doi.org/10.1085/jgp.116.5.653

Takahashi, M.P., and S.C. Cannon. 1999. Enhanced slow inactivation by V445M: a sodium channel mutation associated with myotonia. *Biophys. J.* 76:861–868. https://doi.org/10.1016/S0006-3495(99)77249-8

Todt, H., S.C. Dudley Jr., J.W. Kyle, R.J. French, and H.A. Fozzard. 1999. Ultra-slow inactivation in μ1 Na+ channels is produced by a structural rearrangement of the outer vestibule. *Biophys. J.* 76:1335–1345. https://doi.org/10.1016/S0006-3495(99)77296-6

Vedantham, V., and S.C. Cannon. 2000. Rapid and slow voltage-dependent conformational changes in segment IVS6 of voltage-gated Na(+) channels. *Biophys. J.* 78:2943–2958. https://doi.org/10.1016/S0006-3495(00)76834-2

Wang, S.Y., and G.K. Wang. 1997. A mutation in segment I-S6 alters slow inactivation of sodium channels. *Biophys. J.* 72:1633–1640. https://doi.org/10.1016/S0006-3495(97)78809-X

Wang, S.Y., C. Russell, and G.K. Wang. 2005. Tryptophan substitution of a putative D4S6 gating hinge alters slow inactivation in cardiac sodium channels. *Biophys. J.* 88:3991–3999. https://doi.org/10.1529/biophysj.105.059352

Xiong, W., Y.Z. Farukhi, Y. Tian, D. Disilvestre, R.A. Li, and G.F. Tomaselli. 2006. A conserved ring of charge in mammalian Na+ channels: a molecular regulator of the outer pore conformation during slow inactivation. *J. Physiol.* 576:739–754. https://doi.org/10.1113/jphysiol.2006.115105